



ELSEVIER

Physica C 294 (1998) 183–193

PHYSICA C

The atomic origins of reduced critical currents at [001] tilt grain boundaries in $\text{YBa}_2\text{Cu}_3\text{O}_{7-\delta}$ thin films

N.D. Browning^{a,*}, J.P. Buban^a, P.D. Nellist^{b,1}, D.P. Norton^b, M.F. Chisholm^b,
S.J. Pennycook^b

^a Department of Physics (M / C 273), University of Illinois at Chicago, 845 W. Taylor Street, Chicago, IL 60607-7059, USA

^b Solid State Division, Oak Ridge National Laboratory, P.O. Box 2008, Oak Ridge, TN 37831-6030, USA

Received 9 July 1997; revised 21 August 1997; accepted 22 August 1997

Abstract

Grain boundaries have long been known to have a deleterious and irreproducible effect on the transport properties of high- T_c oxide superconductors, particularly in the high-angle regime where an exponential decrease in critical current has been reported. We demonstrate, through a combination of atomic resolution Z-contrast imaging and bond valence sum analysis, that it is the atomic structure of the grain boundary that dominates this behavior. [001] tilt grain boundaries in thin-film $\text{YBa}_2\text{Cu}_3\text{O}_{7-\delta}$ are composed of arrays of dislocations in defined sequences. The resulting strain fields seriously perturb the local electronic structure, leading to a non-superconducting zone at the grain boundary. The width of this zone increases linearly with misorientation angle, naturally explaining the observed exponential decrease in critical current. In addition, the widely varying J_c measurements for a given grain boundary misorientation can be naturally explained by the faceting of the grain boundary plane. © 1998 Elsevier Science B.V.

Keywords: Grain boundaries; Transport properties; EELS; Z-contrast; STEM

1. Introduction

The transport properties of grain boundaries in $\text{YBa}_2\text{Cu}_3\text{O}_{7-\delta}$ (YBCO), and in particular [001] tilt grain boundaries, have been studied extensively over the last eight years [1–3]. While the reported results for a given misorientation angle can vary substantially, the clear trend is an exponential decrease in

critical current (J_c) with increasing misorientation angle. There have also been many attempts to model the transport properties of boundaries, particularly low-angle boundaries [4–6], but as yet there is no accepted explanation for the exponential decrease from 10–45°. The effects of d-wave symmetry of the superconducting order parameter [7–10] and grain boundary faceting [11–15] may be significant, but can only account for one order of magnitude reduction. The key question therefore still remains as to what effect dominates the critical current behavior of YBCO grain boundaries.

In this paper we use the Z-contrast imaging technique to determine the structures of isolated disloca-

* Corresponding author. Tel.: +1 312 413 8164; Fax: +1 312 996 9016; E-mail: browning@uic.edu

¹ Present address: Cavendish Laboratory, Madingley Road, Cambridge, CB3 0HE, UK.

tion cores in a low-angle [001] tilt boundary and the structure of an asymmetric 30° [001] tilt boundary in YBCO. Using simple bond-valence sum analysis techniques [16–18] the atomic structure is shown to have a dramatic effect on the electronic structure, leading to a non-superconducting boundary core. The boundary structures are similar to those seen in the perovskite SrTiO₃ [19–22] and using the structural unit model [23], the structures of other high-angle boundaries can be predicted. The width of the non-superconducting region in the boundary core is found to increase linearly with misorientation angle. Assuming a direct tunneling model for the current across this non-superconducting region leads to an exponential relationship consistent with the observed experimental transport measurements [1–3]. Simply by considering the non-equilibrium growth conditions for thin films leading to a faceted boundary plane naturally accounts for the scatter in the observed measurements. In addition, this analysis leads to the conclusion that the majority of the reduction in J_c at high-angle grain boundaries is caused by an asymmetric boundary plane. Symmetric boundaries appear to exhibit less change in the electronic structure at the boundary core, consistent with earlier results from electron energy loss spectroscopy (EELS) [24].

2. Experimental techniques and analysis

Atomic structure determinations are made using the high-angle annular dark-field or Z-contrast imaging technique in the scanning transmission electron microscope (STEM) [25–28]. In Z-contrast images, changes in focus and thickness do not cause contrast reversals in the atomic resolution image, thus atomic column sites can be identified unambiguously. Atomic columns at grain boundaries can therefore be located accurately without the need for simulated images; a maximum entropy analysis can be used to obtain column coordinates to $\sim \pm 0.1$ Å accuracy [21,22].

The atomic coordinates can then be used as input for a bond-valence-sum analysis to determine the approximate valence of the copper atoms in the experimental image. Bond-valence sums originate from a concept by Pauling [16], in which the formal valence of a given ion is distributed between its

bonds to its nearest neighbors. The formal valence of an ion is therefore determined primarily by its bond length. This concept has been adapted by Altermatt and Brown [17,18], to provide a simple expression by which the valence of an ion can be determined from its bond length. For the majority of known crystalline structures, the following expression predicts the valence to within 10% of the formal value

$$S = \exp[(r_0 - r_{ij})/B] \quad (1)$$

where r_0 is a constant characteristic of the elements in the bond, B is a constant which is assigned the value 0.37 by fitting to experimental data from a wide range of materials and r_{ij} is the bond length.

In a perfect unit cell of YBCO, the valences of most of the elements involved change very little between YBCO₇ and YBCO₆ (< 10%). The exception to this is copper. In fully oxygenated YBCO the copper (1) valence is ~ 2.3 , whereas in fully oxygen deficient YBCO the copper valence is ~ 1.2 [29], although the copper (2) valence changes by < 10%. This implies that the copper (1) valence can be used as a very sensitive measure of the number of charge carriers present in the structure. To measure the number of charge carriers at grain boundaries in this way, it is obviously critical that the difference in Cu valence between superconducting and non-superconducting states be much greater than the experimental errors in the valence measurement. From the structures observed in the Z-contrast image, the positions of the yttrium, barium, oxygen and copper (2) columns can be adjusted by less than the 0.1 Å error in their location, until they have valences within 10% of their expected values. The copper (1) valence that results is then used to estimate the number of charge carriers present in the actual boundary structure. Note that this analysis assumes that the electronic structure is primarily determined by the copper valence. If this valence is changed by a local structural distortion, or by oxygen doping, we consider the influence on superconductivity to be identical. In fact, we assume always that the structure is fully oxygenated, so that all changes in copper valence here arise from structural disorder. Any oxygen deficiency will only degrade the carrier concentration still further.

For application to YBCO, it has been pointed out that bond-valence calculations are empirical and can-

not be used to determine the valences of the elements involved to better than around 10% accuracy [30]. However, since our atomic positions are only determined to an accuracy of 0.1 Å, errors induced by the bond-valence sum analysis are second order. The bond valence sums are useful indicators of particular atomic positions where a significant change in valence occurs, i.e. the superconducting properties are significantly perturbed. We show that this analysis can give a plausible microscopic explanation for the exponential drop in critical currents with grain boundary misorientation.

3. Results and discussion

Fig. 1 shows a Z-contrast image of a low-angle YBCO grain boundary and Fig. 2 shows a YBCO 30° [001] asymmetric tilt boundary grown by laser ablation on a SrTiO₃ bicrystal substrate.

In the images, the brighter columns consist of Y and Ba atoms, and the less bright columns consist of Cu(1), Cu(2) and O(4) atoms. Columns consisting solely of oxygen atoms, i.e. those containing O(2) or O(1) and O(3) atoms, scatter too little to contribute to the image. The implications of these images for

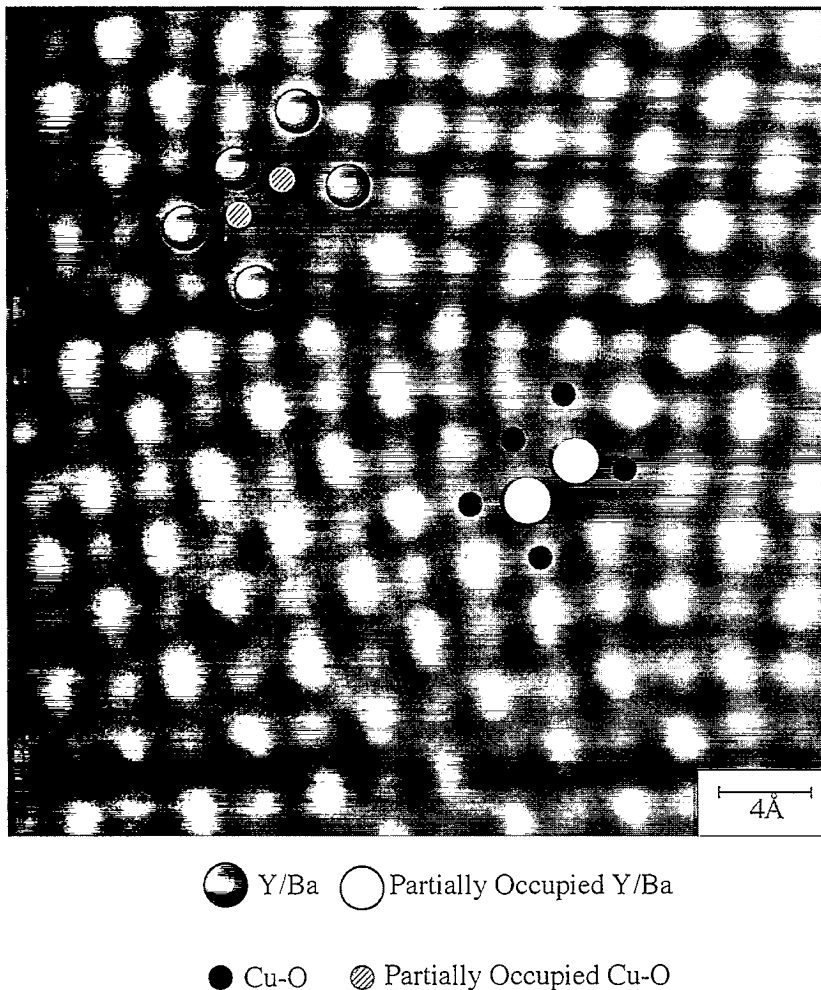


Fig. 1. Z-contrast image of a low-angle [001] tilt boundary in YBCO obtained from a 300 kV VG microscopes HB603 dedicated STEM. The Z-contrast in the image allows the sublattice, i.e. Cu or Y/Ba on which the dislocation core reconstruction forms to be identified.

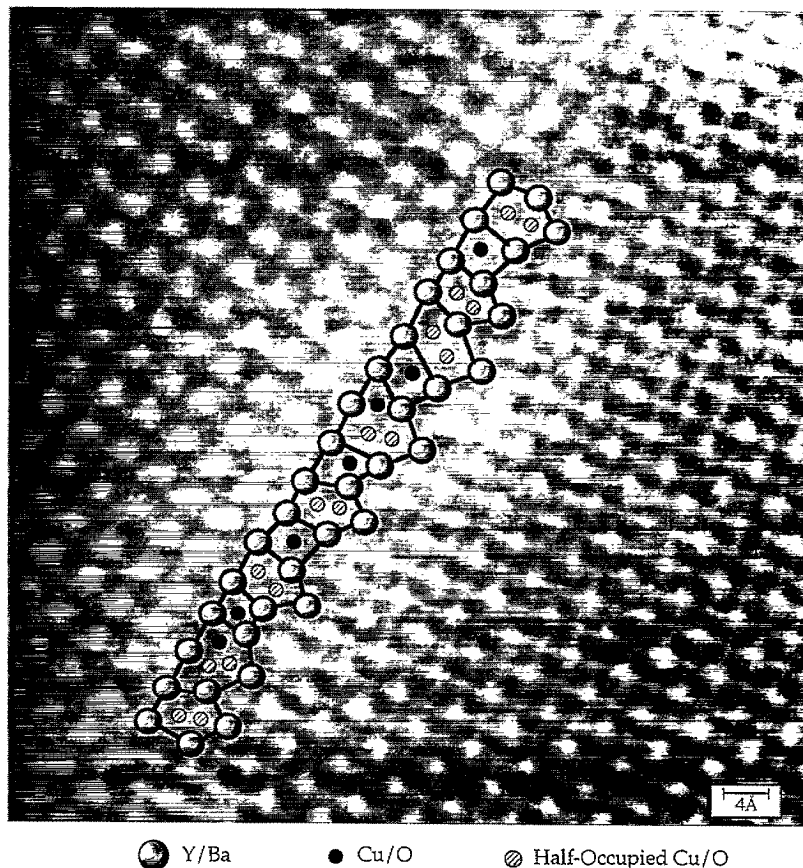


Fig. 2. Z-contrast image of a 30° [001] YBCO tilt boundary obtained from a 300 kV VG microscopes HB603 dedicated STEM.

transport across low- and high-angle grain boundaries is discussed below.

3.1. Low-angle grain boundaries

Low-angle grain boundaries are generally considered to cover the range of misorientations from 0 – 10° . In this regime, the grain boundary plane can be regarded as a linear array of dislocation cores [31], and the strain field around these cores can be calculated from linear elasticity theory [32]. Here, the lattice either side of the grain boundary is assumed to be unstrained and used as a reference for the lattice positions in the vicinity of the dislocation. For [001] tilt boundaries in YBCO, the boundary plane will be composed of dislocation cores with [100] or [010] Burgers vectors, as shown in Fig. 3, (for YBCO the small distortion between the a - and

b -axes needs to be incorporated for quantitative models, but results in no major structural difference between the dislocation cores). However, models based on elasticity theory do not specifically take into account the atomic structure in the dislocation core. The strain is calculated simply by removing a single plane of atoms to create the dislocation core. In addition, for a multicomponent system like YBCO no distinction is drawn between the two possible sublattices, i.e. an [010] dislocation core centered on a copper column or one centered on an yttrium/barium column. Nevertheless, despite lacking a definition of the exact atomic structure in the dislocation core, linear elasticity quantitatively reproduces the critical current behavior of low-angle grain boundaries. In the model by Chisholm and Pennycook [4], a strain of 1% was used as the cut-off between YBCO being superconducting and non-su-

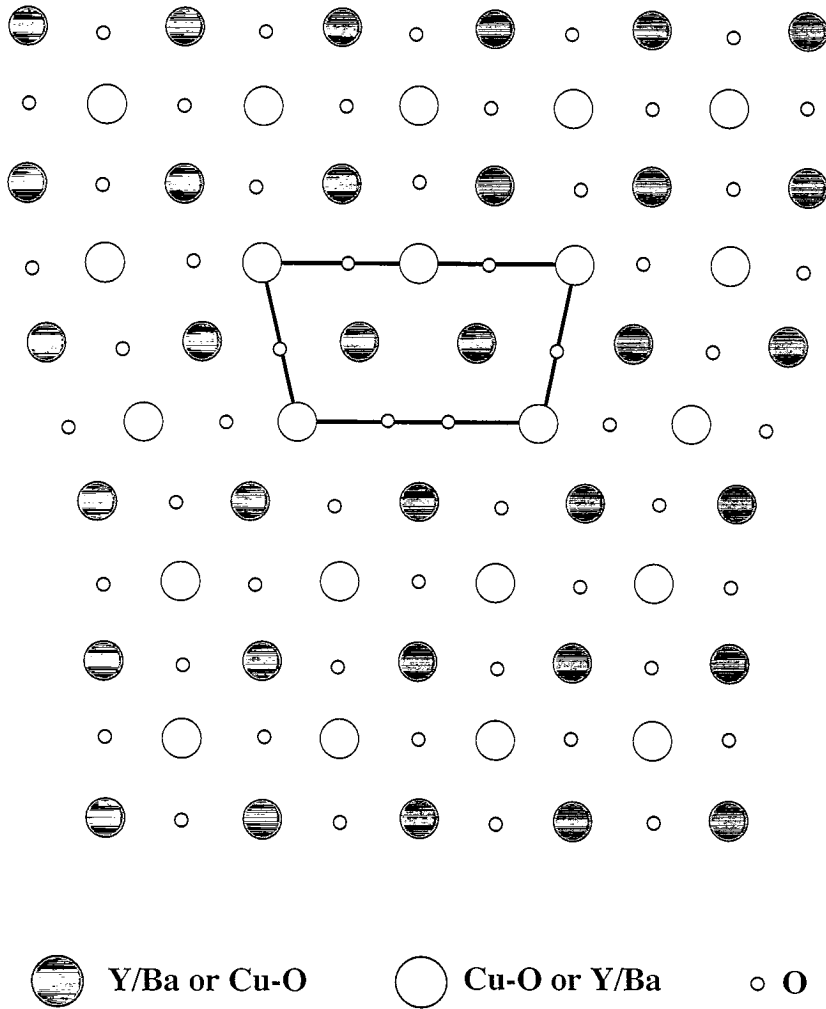


Fig. 3. Schematic of a perfect edge dislocation core in YBCO with a Burgers vector of $[100]$ or $[010]$.

perconducting. This cut-off value was taken from the fact that a 1% strain causes YBCO to be tetragonal and no superconducting phase of YBCO is tetragonal. As the grain boundary misorientation is increased, the separation of the dislocation cores decreases. Hence, progressively more of the grain boundary becomes non-superconducting until at the end of the low-angle regime, the region between dislocation cores where the strain is below 1% becomes comparable to the lattice parameter. At this point it is impossible to use linear elasticity to calculate the grain boundary strain.

The dislocation core structure presented in Fig. 3 is very similar to the structure experimentally observed in Fig. 1, where two distinct dislocation cores in YBCO are shown. In the first case, the dislocation core is constructed from a missing Cu–O plane and in the second case by a missing Y/Ba–O plane. Dislocation cores in low-angle grain boundaries can therefore form on either sublattice. An interesting feature of both cores is that there exist atomic locations where the columns appear too close together. In such situations, like-ion repulsion would be expected to preclude such a structure. However, if we remem-

ber that the Z-contrast image, like any transmission image, is simply a 2-dimensional projection of the 3-dimensional crystal structure, a solution to this problem is for only one of the two sites in each perovskite block to be occupied. If alternate sites are chosen, we would still see two columns in projection but avoid like-ion repulsion. An alternative view of these two 'half-columns' is that they represent a single atomic column that is distorted through the thickness of the crystal in a regular manner, i.e. a 2×1 dislocation core reconstruction.

3.2. High-angle grain boundaries

At the point where the strain fields around dislocation cores begin to overlap, i.e. the end of the low-angle regime, models of grain boundaries based on linear elasticity become inapplicable. At this stage, an alternate methodology to describe the grain boundary structure is by structural units [23]. These structural units are equivalent formally to a dislocation core model of the boundary, and evidence suggests that in the case of the perovskites, they are in fact the same core structures as seen in isolated dislocations [21]. The structural unit model has the advantage that once the structural units have been determined, it is possible to predict the structure of a grain boundary at any misorientation. However, as with the dislocation core model for low-angle boundaries, structural units only define the type of structure that occurs at the grain boundary and on their own cannot provide information on the structure-property relationships.

The structural unit model has been used successfully to predict the structures of grain boundaries in perovskite structured SrTiO_3 bicrystals [18–22]. The structural units observed for SrTiO_3 [001] tilt boundaries are shown in Fig. 4. In a similar manner to the isolated dislocation cores in YBCO, the structural units also appear to contain atomic positions where the cations are too close together. Again, depending on the structural unit, the close separation of the atomic columns can occur for either of the sublattice sites, i.e. the Ti–O columns or the Sr columns.

The bicrystals used in this study are typically used as substrates for the preparation of individual grain boundaries in YBCO thin films [1–3]. The reason that SrTiO_3 is chosen as the substrate for YBCO is primarily due to the closeness of the lattice parameters (3.905 Å for SrTiO_3 compared with $a = 3.81$ Å and $b = 3.88$ Å in YBCO). In view of the fact that YBCO, and for that matter all of the high- T_c superconductors, are closely related to the perovskite structure, it is reasonable to assume that the structure of the YBCO grain boundary would be similar to that of the SrTiO_3 bicrystal. Indeed, in terms of the dislocation core models, the only difference between SrTiO_3 and YBCO is that the Sr columns are replaced by Y/Ba columns and the Ti–O columns are replaced by Cu–O columns. The structure in the [001] projection is the same and the lattice parameter is changed by less than 3%. Therefore, by being able to predict the SrTiO_3 grain boundary structures it should be possible to predict the structure of the thin-film YBCO boundary.

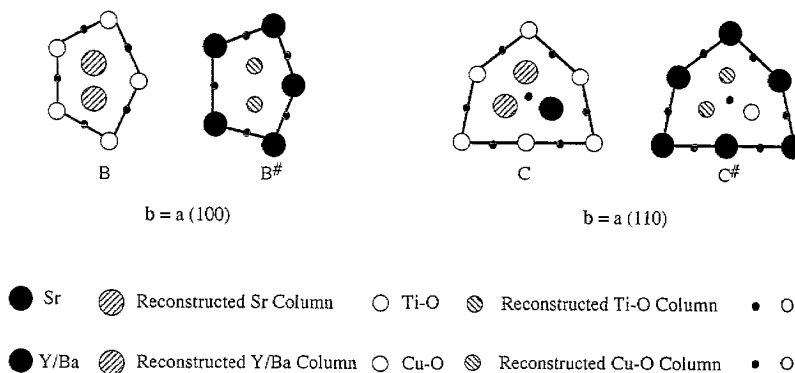


Fig. 4. Structural units identified from a systematic study of [001] tilt boundaries in SrTiO_3 .

This simple argument of course neglects the kinetics of thin film growth. It is well known that YBCO film growth occurs through the nucleation of 3-dimensional islands. The growth of the films takes place in conditions far from equilibrium and, as such, it is hard to imagine a case where the boundary in the film will follow the substrate boundary exactly. This is consistent with TEM observations [11–15] which show the grain boundary plane to meander or facet around the boundary direction defined by the substrate. Such boundaries rarely contain the well defined symmetric structure observed in the bicrystal substrate. In fact, even in the substrate, which is prepared in bulk form and annealed under equilibrium conditions, asymmetric facets are occasionally seen [21,22]. Observations from SrTiO₃ show that these asymmetric facets are composed of a subset of the structural units seen at symmetric grain boundaries, and again occur in well-defined and predictable sequences [21,22]. Only the units with reconstructed Ti–O columns occur on asymmetric boundaries. Therefore a critical difference between asymmetric and symmetric grain boundaries is that

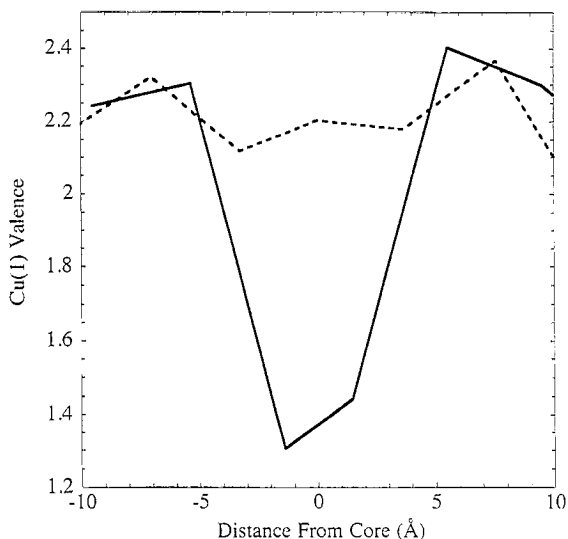


Fig. 5. The change in copper (I) valence as a function of displacement from the dislocation cores with reconstruction on the Cu–O sublattice (—) and the reconstruction on the Y/Ba sublattice (---) shown in Fig. 2. Notice that the dislocation core reconstruction centered on the Cu sublattice shows a valence in the core consistent with non-superconducting YBCO.

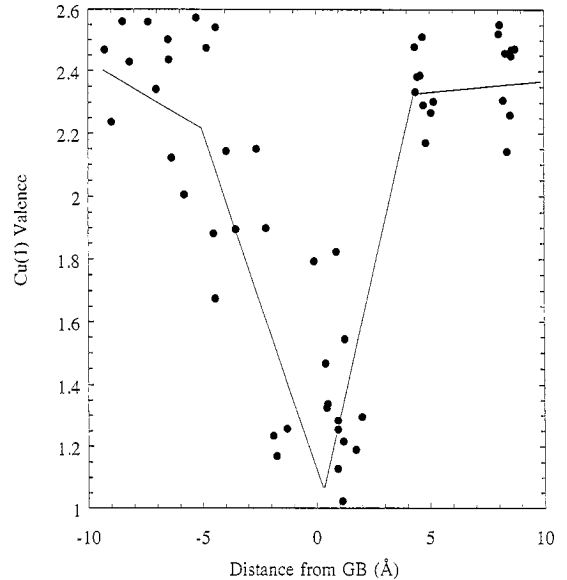


Fig. 6. The change in copper (I) valence as a function of displacement for the 30° asymmetric boundary structure shown in Fig. 2. Notice that in this high-angle regime there are overlapping dislocation cores and the reconstruction leads to a 'wall' of non-superconducting material in the boundary core.

the structural units in asymmetric grain boundaries are centered on only one sublattice.

From the Z-contrast images of the dislocations in YBCO, it is clear that YBCO and SrTiO₃ form the same type of isolated dislocation core structures in low-angle grain boundaries (structural unit B in Fig. 4 is identical to the dislocation core structure (b) in Fig. 1). For high-angle boundaries, the key question is whether there is any relationship between the structure of the faceted YBCO boundary and the structure of the bicrystal boundary. By examining closely the structure of the YBCO asymmetric boundary shown in Fig. 2, we can see the structural units for YBCO are the same as observed for SrTiO₃. In addition, the quasi-periodic repeat of this asymmetric YBCO structure is identical to that constructed using the SrTiO₃ units [33]. For asymmetric YBCO grain boundaries this means the reconstructed atomic columns occur only on the copper sublattice. Therefore, while it is known that the YBCO grain boundary will facet around the orientation of the substrate, the structure of each individual facet can be constructed from the structural units in Fig. 4.

The overall properties of the boundary will then simply be a sum of all the individual facets.

4. Predicting bulk structure–property relationships

Based on these images, it is therefore possible to construct the types of structures that will be present in a YBCO grain boundary for any misorientation angle. However, these models alone cannot provide any information on the properties associated with each structure. To determine the effect of each structure on the transport properties a bond-valence-sum analysis is required.

Analysis of the copper valence around the two dislocation cores in Fig. 1 is shown in Fig. 5 (for all of the other elements, valences are within 10% of the

values expected for perfect unit cells). It is immediately noticeable that the particular sublattice of the dislocation core has a strong effect on the copper valence. Dislocation cores that involve reconstructed copper columns will have a far more deleterious effect on the number of charge carriers than those involving reconstructions on the Y/Ba site. In the case of high-angle grain boundaries, these cores often occur in a continuous sequence, causing a non-superconducting barrier to the flow of current across the boundary. This is the case for asymmetric grain boundaries where all of the structural units contain the reconstruction on the Cu sublattice.

The supposition that asymmetric grain boundaries will have a large carrier depletion zone associated with them is consistent with previous EELS results showing a broad hole-depletion zone [24]. Applying the same bond valence analysis to the 30° boundary

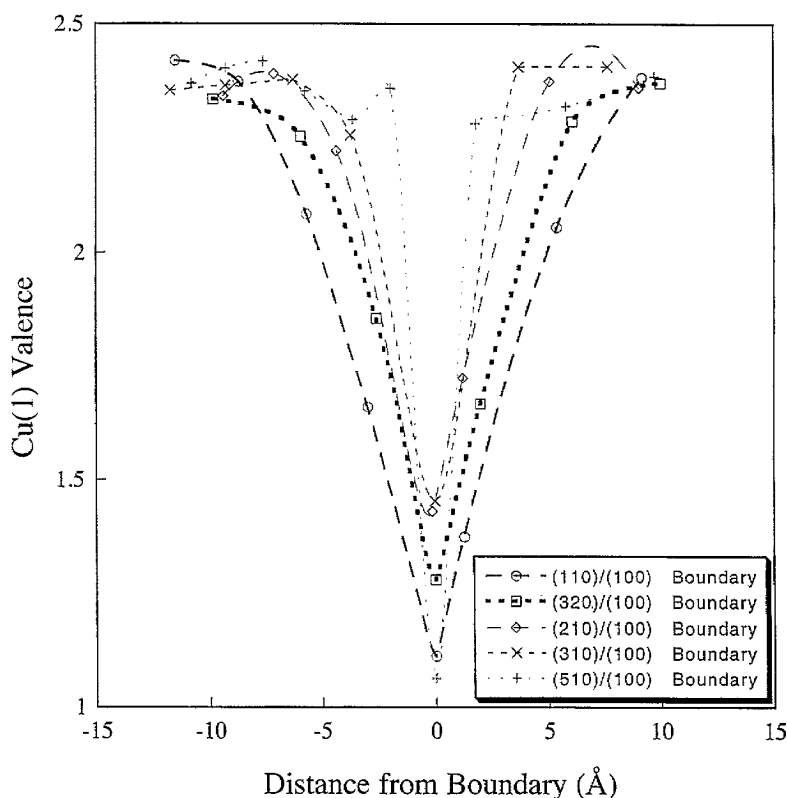


Fig. 7. The change in copper valence as a function of displacement for the 11.4° (boundary plane (100)/(510)), 18.4° (boundary plane (100)/(310)), 26.6° (boundary plane (100)/(210)), 33.7° (boundary plane (100)/(210)), and 45° (boundary plane (100)/(110)) asymmetric boundaries constructed using the structural units of Fig. 4. Notice that the non-superconducting region increases with misorientation angle.

structure shown in Fig. 3, confirms that there is a broad non-superconducting region at the boundary (Fig. 6). To investigate this effect further, the structures of asymmetric boundaries at other misorientation angles were constructed from the structural units. As a first approximation the boundaries were considered to be straight, i.e. consist of one particular grain boundary plane. For boundary misorientations of 11.4° (boundary plane (100)/(510)), 18.4° (boundary plane (100)/(310)), 26.6° (boundary plane (100)/(210)), 33.7° (boundary plane (100)/(210)), and 45° (boundary plane (100)/(110)), the copper (1) valence as a function of distance from the boundary core can then be calculated from bond-valence sum analysis. In Fig. 7, the valence of each copper (1) site is plotted against its distance from the boundary. Again, it is clear from this plot that the boundary perturbs the local electronic structure sufficiently to create a non-superconducting zone, but more importantly, it is seen that the width of this zone increases with misorientation angle. These plots can now be used to define a grain boundary width. We assume a square well model with a non-superconducting zone of width Δ between fully superconducting grains. Fig. 8 shows the variation in grain boundary width as a function of misorientation angle

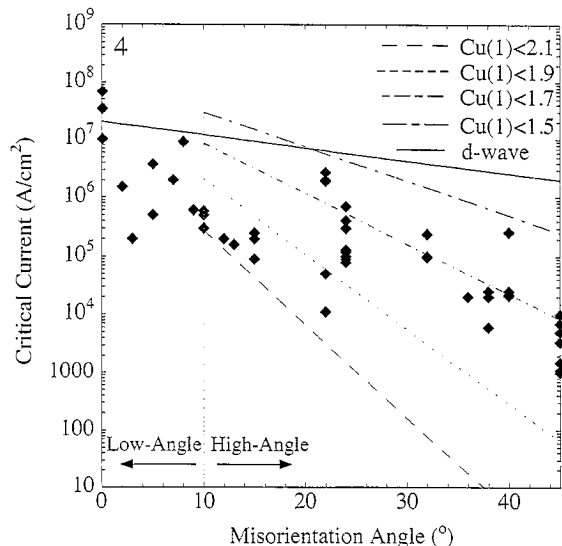


Fig. 9. Experimental observations of J_c ($T = 4.2$ K) as a function of misorientation angle taken from the results of several groups [1–3] (○) show an exponential dependence. In cases where the results were reported at $T = 77$ K, the values at 4.2 K were extrapolated from the temperature dependence of J_c [36]. The grain boundary tunneling current calculated from Eq. (1) using the grain boundary widths from Fig. 8 shows excellent quantitative agreement for a width defining Cu(1) valence of between 1.5 and 1.9. This copper valence corresponds to the Cu(1) valence in bulk YBCO when it becomes non-superconducting. The predicted drop in J_c due to the symmetry of the superconducting order parameter is insufficient to account for the observed behavior.

using different Cu(1) valences to define the width Δ . It is clear from the plot that whatever criterion is used to define boundary width, the width increases with misorientation angle.

The majority of the copper sites in all asymmetric grain boundaries are therefore non-superconducting. As was stated earlier, for thin films of YBCO grown on bicrystal substrates, the boundaries facet with predominantly asymmetric boundary planes. It is therefore reasonable to assume that the experimental transport measurements across high-angle grain boundaries were dominated by transport across these asymmetric facets. At these boundaries the current must flow by tunneling across the non-superconducting barrier. The magnitude of the tunneling current across a barrier can be calculated from [34]

$$J_c = J_{c0} \exp(-2\kappa\Delta) \quad (2)$$

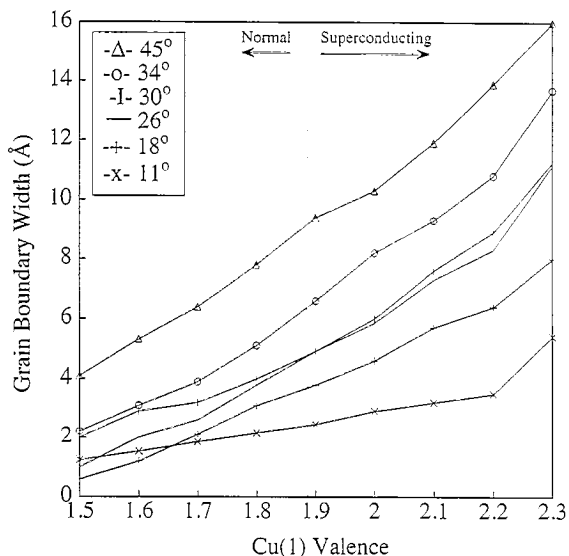


Fig. 8. Width of the non-superconducting region as a function of the defined cut-off in Cu(1) valence for the boundaries in Figs. 6 and 7.

where J_{c0} is the bulk critical current, Δ is the interface width and κ is the decay constant (7.7/nm) [34,35]. For each of the grain boundaries above, the width can be used to determine the expected tunneling current for a constant applied voltage, the criterion used experimentally to measure critical currents. In Fig. 9, the tunneling current as a function of misorientation angle for asymmetric boundaries is plotted and compared with a range of experimental critical current measurements [1–3]. For the boundary widths defined above, the structural unit model quantitatively reproduces the trend of exponentially decreasing critical current with increasing misorientation angle, and lies well within the range of experimental results. For comparison, the critical current behavior predicted by the d-wave symmetry of the superconducting order parameter is also shown in Fig. 9.

The large variability in the J_c measurements shown in Fig. 9 is also naturally explained by the structural unit model. TEM studies have shown the universal presence of facets in thin film grain boundaries, which typically occur on length scales in the region of 10–100 nm. Each of these facets corresponds to a different grain boundary plane which will be characterised by a given set of structural units and will have an associated grain boundary width. The bulk scale J_c measurements therefore represent the sum of all facets whose individual behavior can be predicted from the structural unit model. As the growth of thin films is a non-equilibrium process, the range of boundary structures will be extremely sensitive to the growth parameters. This leads to the variability in measurements of J_c and the $J_c \rho_n$ product, as well as a smoothing of the macroscopic current–voltage characteristics. Predictions of grain boundary properties must therefore take into account the degree of facetting that occurs in a given growth process.

5. Conclusions

Obtaining atomic coordinates directly from Z-contrast images, and performing bond valence sum analyses can provide significant insights into the microscopic origin of superconducting transport properties. We have shown how the structural distortion around

the dislocation cores comprising a 30° [001] bicrystal tilt grain boundary leads to a continuous non-superconducting zone. By constructing models for boundaries of other orientations, and relaxing the coordinates by bond valence sum analysis, we show that the width of the non-superconducting zone increases almost linearly with increasing grain boundary misorientation, and can therefore explain the exponential reduction in critical current reported in the literature. Using realistic criteria for the width of this zone explains the three orders of magnitude reduction seen experimentally. Models based on the possible d-wave symmetry of the order parameter cannot be the dominant cause of such a reduction, although may result in additional effects. Similarly, oxygen deficiency at the boundary will also further degrade the transport across the boundary by increasing the width of the non-superconducting zone. In fact, due to the extreme sensitivity of the tunnelling current to the width of this zone, we would naturally expect that the actual critical currents measured experimentally would be very sensitive to the exact growth and processing conditions. This we believe is the origin of the large scatter in the experimental data seen in Fig. 9, and is entirely consistent with our microscopic model. This could be simply quantified by removing some of the mobile oxygens from the vicinity of the boundary core, and recalculating the bond valence sums to obtain the new width of the non-superconducting zone.

Our approach has highlighted clear differences between structural units containing reconstructed atomic columns on different sublattice sites. In particular, it has been found that for reconstruction on the copper sublattice there is a broad region in which there is a suppression of the carrier concentration. This reconstruction occurs at all asymmetric grain boundaries, and such boundaries are common in thin-film YBCO because of the tendency for one grain to facet on the {100} plane. An interesting aspect of this result is that it predicts that symmetric grain boundaries should have better J_c behavior than asymmetric boundaries. The symmetric grain boundaries contain reconstructions predominantly on the Y/Ba sites (Fig. 5), and as such there should be unperturbed Cu sites at the boundary. This could explain the EELS observations from the symmetric 36° grain boundaries that show no hole depletion

[24], as well as the anomalously high J_c measurements from certain high-angle symmetric boundaries in thin film YBCO [37]. The reconstructed columns also represent ideal positions for the substitution of dopant atoms, which may be able to correct the copper valence and restore the carrier concentration. Obviously such mechanisms require extensive further study, but in principle they could lead to a fundamental understanding of the atomic scale behavior of grain boundaries. This understanding may in turn aid the production of wires with greater current carrying capacity, and facilitate tailoring of boundary structures for applications such as superconducting quantum interference devices (SQUIDs).

Acknowledgements

We would like to thank J.T. Luck for the preparation of the samples used for this work, and J. Halbritter and Z. Ivanov for valuable comments. This research was sponsored by the National Science Foundation under grant No. DMR-9503877 and by the Division of Materials Sciences, US Department of Energy, under contract No. DE-AC05-96OR22464 with Lockheed Martin Energy Research Corporation, and by appointment to the ORNL Postdoctoral Research Program administered jointly by ORNL and ORISE.

References

- [1] D. Dimos, P. Chaudhari, J. Mannhart, Phys. Rev. B 41 (1990) 4038.
- [2] R. Gross, B. Mayer, Physica C 180 (1990) 235.
- [3] Z.G. Ivanov et al., Appl. Phys. Lett. 59 (1990) 3030.
- [4] M.F. Chisholm, S.J. Pennycook, Nature 351 (1991) 47.
- [5] K. Jagannadham, J. Narayan, Mater. Sci. Eng. B 26 (1994) 75.
- [6] D. Agassi, C.S. Pande, R.A. Masumura, Phys. Rev. B 52 (1995) 16237.
- [7] H. Hilgenkamp, J. Mannhart, B. Mayer, Phys. Rev. B 53 (1996) 14586.
- [8] C.C. Tsuei et al., Phys. Rev. Lett. 73 (1994) 593.
- [9] D.A. Wollman et al., Phys. Rev. Lett. 71 (1993) 2134.
- [10] J.H. Miller et al., Phys. Rev. Lett. 74 (1995) 2347.
- [11] C.L. Jia et al., Physica C 196 (1992) 211.
- [12] A.F. Marshall, C.B. Eom, Physica C 207 (1993) 239.
- [13] C. Traeholt et al., Physica C 230 (1994) 425.
- [14] B. Vuchic et al., Mat. Res. Soc. Symp. Proc. 357 (1995) 419.
- [15] B. Kabius et al., Physica C 231 (1994) 123.
- [16] L. Pauling, J. Am. Ceram. Soc. 51 (1929) 1010.
- [17] D. Altermatt, I.D. Brown, Acta Crystallogr. B 41 (1985) 240.
- [18] I.D. Brown, D. Altermatt, Acta Crystallogr. B 41 (1985) 244.
- [19] M.M. McGibbon, N.D. Browning, M.F. Chisholm, A.J. McGibbon, S.J. Pennycook, V. Ravikumar, V.P. Dravid, Science 266 (1994) 102.
- [20] N.D. Browning, S.J. Pennycook, M.F. Chisholm, M.M. McGibbon, A.J. McGibbon, Interface Sci. 2 (1995) 397.
- [21] N.D. Browning, S.J. Pennycook, J. Phys. D 29 (1996) 1779.
- [22] M.M. McGibbon, N.D. Browning, A.J. McGibbon, S.J. Pennycook, Phil. Mag. A 73 (1996) 625.
- [23] A.P. Sutton, V. Vitek, Proc. Roy. Soc. London A 309 (1983) 1.
- [24] N.D. Browning, M.F. Chisholm, S.J. Pennycook, D.P. Norton, D.H. Lowndes, Physica C 212 (1993) 185.
- [25] S.J. Pennycook, L.A. Boatner, Nature 336 (1988) 565.
- [26] S.J. Pennycook, D.E. Jesson, Phys. Rev. Lett. 64 (1990) 938.
- [27] D.E. Jesson, S.J. Pennycook, Proc. Roy. Soc. London A 449 (1995) 273.
- [28] R.F. Loane, P. Xu, J. Silcox, Ultramicroscopy 40 (1992) 121.
- [29] I.D. Brown, J. Solid State Chem. 82 (1989) 122.
- [30] L. Jansen, R. Block, Physica C 181 (1991) 149.
- [31] W.T. Read, W. Shockley, Phys. Rev. 78 (1950) 275.
- [32] J.P. Hirth, J. Lothe, Theory of Dislocations, Wiley, New York, 1982.
- [33] A.P. Sutton, Acta Metall. 36 (1988) 1291.
- [34] J. Halbritter, Phys. Rev. B 46 (1992) 14861.
- [35] H.L. Edwards et al., Phys. Rev. Lett. 69 (1992) 2967.
- [36] J. Mannhart et al., Phys. Rev. Lett. 61 (1988) 2476.
- [37] Z.G. Ivanov, private communication.